JOURNAL OF COMPUTATIONAL PHYSICS 29, 219–236 (1978)

A Multidimensional Quasineutral Plasma Simulation Model

D. W. HEWETT AND C. W. NIELSON

Los Alamos Scientific Laboratory, University of California, Los Alamos, New Mexico 87545

Received July 27, 1977; revised February 23, 1978

A multidimensional hybrid simulation model has been developed for use in studying plasma phenomena on extended time and distance scales. The model makes fundamental use of the small Debye length or quasineutrality assumption. The ions are modeled by particle-in-cell techniques, while the electrons are considered a collision-dominated fluid. Some electron inertial effects are retained. The fields are calculated in the nonradiative Darwin limit. The quasineutral counterpart of Poisson's equation is obtained by first summing the electron and ion momentum equations and then taking the quasineutral limit. The resulting elliptic equation correctly includes those electrostatic potentials which occur in sheath or ambipolar phenomena while neglecting the short-range electrostatic fields which give rise to plasma oscillations. This model has been implemented in a two-dimensional code QN2. A lower hybrid drift unstable equilibrium with parameters accessible to both hybrid and full-particle simulation has been selected as a test of the code and a demonstration of the model. Initial results indicate quite good agreement between the two simulation methods in linear growth rate and wave number.

1. INTRODUCTION

Plasmas of interest in thermonuclear research are often characterized by parameters which lie intermediate between those which make a magnetohydrodynamic (MHD) model adequate and those which demand a full Vlasov treatment. In this hybrid regime, the density, temperatures, and magnetic field are such that the ions are essentially collisionless and have trajectories in position space which cause them to experience large variations in both electromagnetic fields and density; this requires a Vlasov treatment of the ions. On the other hand, the electrons may experience orders of magnitude more collisions than do the ions or have relatively small Larmor orbits. The electron behavior may then be adequately modeled by treating electrons as a collision-dominated thermal fluid. The application of MHD models or full Vlasov models in this regime will be with questionable validity for MHD models and excessive computational cost for full Vlasov models.

Several techniques, both analytical and numerical, have been proposed to model plasma behavior in this hybrid parameter regime. These fall into two classes depending on which of the two small quantities in the hybrid plasma regime is chosen as the expansion parameter. One approach assumes that the electron Larmor radius r_{ce} is vanishingly small compared to scale lengths of interest. This is the premise of electron guiding center models [1] as well as the drift-kinetic analytic model of D'Ippolito and

0021-9991/78/0292-0219$02.00/0

Davidson [2]. Such methods are naturally well suited to low-β plasma phenomena in which strong magnetic fields insure the validity of the small r_{ce} assumption. Limitations are encountered, however, when approaching zero magnetic field in a high-β plasma.

The second general method used to develop a hybrid model is to assume that the Debye length λ_D is small compared to other scale lengths of interest in the problem. The assumption of small λ_D is equivalent to assuming quasineutrality since plasmas deviate from charge neutrality only on distance scales small compared to a Debye length. The Vlasov-fluid model of Freidberg [3] features a fully kinetic treatment of the ions coupled with a massless, cold, neutralizing electron fluid which moves according to the prescription $\mathbf{E} = \mathbf{u}_e \times \mathbf{B}$. This model has been used primarily to ascertain the finite Larmor radius stabilization of global MHD modes [4, 5]. Gerwin has extended the model to include finite electron temperature effects [6].

Quasineutral hybrid plasma models have been the bases of several quite productive one-dimensional simulation codes. While early treatments of θ-pinch implosions used full fluid codes [7, 8], the importance of ion reflection in such implosions was recognized; proper treatment of this phenomenon requires a Vlasov treatment of the ions. Nielson and Sgro [9] developed a one-dimensional hybrid code which uses a particle-in-cell technique for the ions coupled with a massless electron fluid to study the behavior of a variety of implosion-heated devices. Hamasaki and Krall [10] have also developed and applied a one-dimensional hybrid model which treats implosion phenomena in high-β θ-pinches. The earliest two-dimensional hybrid code implementing a quasineutral model was reported by Shonk and Morse [11]. Recently, Byers *et al.* [12] have developed a quasineutral hybrid model which has been applied in one dimension and is intended for two-dimensional applications.

Each of these codes makes fundamental use of zero mass electrons in the field calculation. The essential feature of hybrid codes exploiting the small electron mass condition is that in this limit the electron momentum equation can be used in combination with Maxwell's equations as part of the field calculation. The electron current is then deduced from the most recently calculated fields; only the ion component of the current explicitly contributes to the field-equation source terms.

Previous hybrid codes retaining electron inertia in one dimension have been described by Forslund and Freidberg [13], who applied their code to the study of collisionless shocks and to θ-pinch implosions, and by Liewer [14], whose code was used to study the ion–ion streaming instability in an imploding pinchlike plasma. The hybrid model described here is the multidimensional generalization of these models. It makes use of quasineutrality and retains some aspects of finite electron mass. The transverse or divergence-free part of the electron current remains a fundamental part of the time integration scheme. The retention of finite electron mass allows this model to display many phenomena which require finite electron cyclotron frequency. In addition, for those applications with small electron–ion collision frequency, sheaths comparable in thickness to the collisionless skin depth c/ω_{pe} may be studied.

The electron representation in our model is based on the assumed ordering of collision frequencies $\nu_{ee} \gg \nu_{ei} \gg \nu_{ii}$ so that the electron component can be treated as a

collision-dominated thermal fluid while the ions are represented by the collisionless particle-in-cell technique. The fields are calculated in the radiationless Darwin limit [15]—an instantaneous propagation model in which the Lagrangian is correct to order $(v/c)^2$. The time integration algorithm can therefore follow the traditional method of advancing the plasma source terms and then calculating the instantaneous electric and magnetic fields consistent with these sources.

Several new techniques have been developed for this multidimensional synthesis of hybrid and Darwin models [16, 17]. The most important requirement was that high-frequency electron plasma oscillations not be followed in detail, thus allowing the maximum time step to be much larger than ω_{pe}^{-1}. This feature implies that the strong coupling between the longitudinal (curl-free) part of the electric field and the electron current must be removed. The decoupling is accomplished by the requirement that part of the electron current be determined by the quasineutral continuity equation

$$\nabla \cdot (\mathbf{J}_i + \mathbf{J}_e) = 0 \tag{1}$$

which for suitable boundary conditions completely determines the longitudinal or curl-free part of the electron current from the ion current. Solving for the time-advanced longitudinal electron current directly from the advanced ion current thus obviates the need for using the longitudinal part of the electron momentum equation and the strong short-range coupling between longitudinal parts of the electron current and electric field is excluded. In one dimension this decoupling is easily implemented because of the fact that all divergence-free current is normal to the direction of variation and all curl-free current is along the direction of variation.

A new technique is required to determine the longitudinal electric field (or equivalently the electrostatic potential) consistent with the quasineutral assumption. Exact charge neutrality would of course require the electrostatic field to be identically zero. Quasineutrality implies only that the difference between the ion and electron charge densities be everywhere small in a relative sense. In any equation in which the electron density n_e appears, quasineutrality implies that the change introduced by substituting the ion density n_i for n_e is negligibly small. This condition is found in plasmas which exhibit macroscopic inhomogeneities and require long-range electrostatic potentials for consistency. Common examples include the radial implosion and containment of θ-pinches and axial containment schemes for mirror devices requiring ambipolar potentials. As will be fully discussed later, a quasineutral "Poisson" equation can be obtained using only the quasineutral continuity Eq. (1) and the sum of the electron and ion momentum equations. The solution of the resulting elliptic equation of the form

$$\nabla \cdot (\mu \nabla \phi) = \chi \tag{2}$$

produces the required longitudinal electric fields consistent with the small λ_D assumption.

A brief description of the ion particle-in-cell methodology is presented in Section 2. Section 3 presents the mathematical treatment of the electron fluid followed by a discussion of the quasineutral Darwin model field calculations in Section 4. Since the

main purpose of hybrid code development has been to model plasma phenomena on truly macroscopic time and length scales, Section 5 deals with the mechanisms through which the plasma model interacts with external influences. Finally, a two-dimensional comparison between full particle-in-cell and hybrid simulation techniques is presented in Section 6. The test case is a strongly inhomogeneous lower hybrid drift unstable equilibrium [18].

2. Ions

The ion component of the simulated plasma is modeled by representing the ion distribution with a discrete set of particles. Associated with each particle are a mass, a charge, two position coordinates, and three velocity coordinates. By initializing these particles in velocity and position with appropriate weight factors, arbitrary low-order velocity moments of the ion distribution can be represented. The ion distribution is advanced in time by stepping forward in time each particle under the influence of the local self-consistent Lorentz force using particle-in-cell techniques. Following Nielson and Lewis [15], the particle-stepping algorithm is based upon the following equations which are second-order accurate in the time step Δt. Explicitly,

$$\mathbf{v}^0 = \mathbf{v}^{-1/2} + \tfrac{1}{2}hE^0, \tag{3}$$

$$\mathbf{v}^{1/2} = f\mathbf{v}^{-1/2} + h(\mathbf{E}^0 + g\mathbf{B}^0 + \mathbf{v}^0 \times \mathbf{B}^0), \tag{4}$$

$$\mathbf{x}^1 = \mathbf{x}^0 + \Delta t\, \mathbf{v}^{1/2}, \tag{5}$$

where $h = q\,\Delta t/m$, $f = 1 - (\frac{1}{2}h^2)(\mathbf{B}^0)^2$, and $g = \frac{1}{2}h(\mathbf{v}^{-1/2} \cdot \mathbf{B}^0)^2$. The accuracy of $\mathbf{v}^{1/2}$ and $\mathbf{x}^1$ is of order Δt^2 so that the accumulated error is of order Δt. At the end of each time step, the required velocity moments of the ion distribution are calculated by averaging over the new positions and velocities of the particles. Since the simulation model is to calculate the fields in the Darwin limit, the divergence $\mathbf{K}_i$ of the ion kinetic energy tensor is necessary in addition to the normally required density n_i and current $\mathbf{J}_i$. Numerical details of this extension of the particle-in-cell technique can be found in the original reference of Nielson and Lewis.

3. Electron Fluid

The electron component of the simulated plasma is considered to be a neutralizing thermal fluid. Consequently, the electron density n_e is nearly indistinguishable from the newly obtained ion density n_i and will be considered equal to n_i to lowest order in expressions requiring n_e. One consequence of this assumption is displayed by considering the continuity equation,

$$e\frac{d}{dt}(n_i - n_e) + \nabla \cdot (\mathbf{J}_i + \mathbf{J}_e) = 0, \tag{6}$$

where n_i and n_e are the ion and electron densities and $\mathbf{J}_i$ and $\mathbf{J}_e$ are the ion and electron currents. Since n_i is considered equal to n_e, the continuity equation reduces to

$$\nabla \cdot \mathbf{J}_e = -\nabla \cdot \mathbf{J}_i . \tag{7}$$

To exploit the consequences of Eq. (7), the electron current J_e is decomposed into longitudinal (irrotational) $\mathbf{J}_{el}$ and transverse (solenoidal) $\mathbf{J}_{et}$ parts.

$$\mathbf{J}_e = \mathbf{J}_{el} + \mathbf{J}_{et} . \tag{8}$$

These two components are defined by

$$\nabla \cdot \mathbf{J}_{el} = \nabla \cdot \mathbf{J}_e , \tag{9}$$

$$\nabla \times \mathbf{J}_{el} = 0, \tag{10}$$

$$\nabla \cdot \mathbf{J}_{et} = 0, \tag{11}$$

$$\nabla \times \mathbf{J}_{et} = \nabla \times \mathbf{J}_e . \tag{12}$$

The subscript l will hereafter indicate the irrotational or curl-free component and the subscript t will denote the transverse or divergence-free component. The terms "longitudinal" and "transverse" have been used in the text to conform to standard usage. The reader is cautioned to avoid the confusion that often arises due to the connotation of direction associated with these terms. These terms denote vector properties; they can imply direction only in geometrically limited special cases.

Since $\mathbf{J}_{el}$ is longitudinal, it may be obtained by taking the gradient of a scalar potential V,

$$\mathbf{J}_{el} = -\nabla V, \tag{13}$$

where V is governed by a Poisson equation obtained by substituting Eq. (13) into Eq. (9). Combining this result with Eq. (7), the potential V is obtained from

$$\nabla^2 V = \nabla \cdot \mathbf{J}_i . \tag{14}$$

Equations (13) and (14) uniquely determine $\mathbf{J}_{el}$ when the appropriate boundary conditions on V are given for Eq. (14). Boundary conditions are reviewed in Section 5. For purposes of the present discussion, periodic and/or Neumann (from a prescribed normal component of $\mathbf{J}_{el}$) boundary conditions will suffice to provide a unique solution. These procedures described by Eqs. (13) and (14) allow the longitudinal part of the electron current to be obtained from the ion current. The longitudinal electron current $\mathbf{J}_{el}$ therefore cannot exhibit faster temporal behavior that experienced by the ions (assuming the boundary conditions do not themselves vary on a faster time scale).

The transverse part of the electron current is advanced explicitly in time by direct evaluation of the electron momentum equation

$$\dot{\mathbf{J}}_e = \mathbf{K}_e + \frac{q^2}{m_e} n_e \mathbf{E} + \frac{q}{m_e c} \mathbf{J}_e \times \mathbf{B} + \nu_{ei}(\mathbf{J}_i + \mathbf{J}_e), \tag{15}$$

where ν_{ei} is the electron–ion collision frequency and $\mathbf{K}_e$ is the divergence of the electron kinetic energy tensor

$$\mathbf{K}_e = -q\nabla \cdot \int \mathbf{v}\mathbf{v} f_e \, d^3v \tag{16}$$

in which f_e is the electron distribution function. After calculation of the vector field $\dot{\mathbf{J}}_e$, the transverse part $\dot{\mathbf{J}}_{et}$ can be obtained by subtracting the longitudinal part

$$\dot{\mathbf{J}}_{et} = \mathbf{J}_e - \dot{\mathbf{J}}_{el} . \tag{17}$$

$\dot{\mathbf{J}}_{el}$ is determined by mathematical methods analogous to those used to find $\mathbf{J}_{el}$. In effect, the methods reduce to

$$\dot{\mathbf{J}}_{et} = \dot{\mathbf{J}}_e + \nabla V, \tag{18}$$

where

$$\nabla^2 V = -\nabla \cdot \dot{\mathbf{J}}_e . \tag{19}$$

As before, external influences on the electron current must be considered when choosing the boundary conditions for V in Eq. (19). Knowledge of the normal component of $\dot{\mathbf{J}}_{el}$ on the boundaries of the simulation region is sufficient to determine uniquely the time rate of change of the vector $\mathbf{J}_{et}$ given $\dot{\mathbf{J}}_e$ from Eq. (15). The implications of this choice for boundary conditions of Eq. (19) are further discussed on Section 5.

The time advance of $\mathbf{J}_{et}$ is accomplished as follows. First, the temporary vector $\mathbf{J}_{es}$ is defined by

$$\mathbf{J}_{es} = \mathbf{J}_{el}^{n} + \mathbf{J}_{et}^{n-1/2}. \tag{20}$$

Now the transverse current may be advanced by the two steps

$$\mathbf{J}_e^{n} = \mathbf{J}_{es} + 0.5\Delta t \, [\dot{\mathbf{J}}_e(\mathbf{K}_e^{n}, n_e^{n}, \mathbf{E}^{n}, \mathbf{J}_{es}, \mathbf{B}^{n})]_t , \tag{21}$$

$$\mathbf{J}_{et}^{n+1/2} = \mathbf{J}_{et}^{n-1/2} + \Delta t \, [\dot{\mathbf{J}}_e(\mathbf{K}_e^{n}, n_e^{n}, \mathbf{E}^{n}, \mathbf{J}_e^{n}, \mathbf{B}^{n})]_t \tag{22}$$

in which each evaluation of $\dot{\mathbf{J}}_e$ is obtained from Eq. (15). The superscript n refers to the relative position in time of the quantities. This scheme is second-order accurate in Δt; Eq. (21) advances the transverse part of the electron current the additional one-half time step required so that the result of Eq. (21) is the total electron current at time n. Use of this current to evaluate the current time derivative in Eq. (22) produces second-order accuracy by virture of time centering.

Equation (22) has proven to be sensitive to details of differencing. Relatively straightforward differencing leads to a slowly growing alternate-cell (Lax-type) instability which causes diffusion of the gradients in the problem. By applying diagonal cell averaging of the longitudinal electric field prior to its use in Eq. (22), the diffusion has been substantially reduced. Further study of the cause and correction of this numerical instability is needed.

From the discussion following Eq. (14), it is apparent that the characteristic time scales of $\mathbf{J}_{el}$ are the same as that of the ions. This result is consistent with and required by quasineutrality. The characteristic time scales for $\mathbf{J}_{et}$ are also not in any way affected by electron plasma oscillations because the interaction of E_l and $\mathbf{J}_{el}$ has been excluded except indirectly through the ion motion. By deducing the electrostatic field from a quasineutral Poisson equation (as described in the following section) electron plasma oscillation variations in the electrostatic field are suppressed. Electron inertia *is* retained in the transverse part of the electron current and, consequently, any phenomenon that requires a finite mass ratio m_i/m_e and that does not require unbalanced charge is still included in this model. Retention of the electron mass in the transverse component does necessitate following electron cyclotron motion when there is a component of the magnetic field in the simulation plane (see appendix). For high-β plasmas, this is not a major restriction and is in fact required for some problems of present interest.

In addition to the fields, density, and currents, the evaluation of $\dot{\mathbf{J}}_e$ using Eq. (15) requires the divergence $\mathbf{K}_e$ of the electron kinetic energy tensor given by Eq. (16). For this purpose, the electron distribution shall be assumed to have the following form:

$$f_e(x, y, \mathbf{v}, t) = \left(\frac{2\pi T_e}{m_e}\right)^{-3/2} n_e \exp\left(\frac{-m_e(\mathbf{v}-\mathbf{u}_e)^2}{2T_e}\right), \tag{23}$$

where the density n_e, the electron drift velocity $\mathbf{u}_e$, and the isotropic electron temperature T_e are functions of both position and time [19]. Thus, the velocity dependence of the electrons can be no more complicated than a drifting Maxwellian of arbitrary width. This assumption is equivalent to an equation of state for the electron fluid; it closes the set of moment equations needed to describe the electrons. The expression for $\mathbf{K}_e$ found by substituting Eq. (23) into Eq. (16) is

$$\mathbf{K}_e = -q\nabla \cdot \left(\frac{n_e T_e}{m_e}\mathbf{I} + n_e \mathbf{u}_e \mathbf{u}_e\right), \tag{24}$$

where $\mathbf{I}$ is the identity tensor and $\mathbf{u}_e\mathbf{u}_e$ is a dyadic.

The electron temperature T_e necessary for the evaluation of Eq. (24) is advanced in time by direct application of the thermodynamic relation for the specific entropy s [20],

$$\frac{ds}{dt} = \frac{1}{n_e T_e}\frac{dq}{dt} \tag{25}$$

in which dq/dt is the heat production rate per cell, the most often used example being Ohmic heating $dq/dt = \eta \mathbf{J}^2$. The specific entropy of the electron distribution given by Eq. (23) is

$$s = \alpha - \ln(n_e T_e^{-3/2}), \tag{26}$$

where α is a constant. Combining Eqs. (25) and (26), the relation giving the time rate of change of T_e is

$$\frac{\partial T_e}{\partial t} = \frac{T_e}{3} \nabla \cdot \mathbf{u}_e - \nabla \cdot (\mathbf{u}_e T_e) + \frac{2}{3n_e}\left[\frac{dq}{dt} + T_e R\right], \tag{27}$$

where R is a source term for electrons representing the net rate at which electrons are generated or introduced.

It should be noted that naive numerical differencing in Eqs. (24) and (27) can possibly result in an unsatisfactory algorithm [21–23]. Numerical evaluation of expressions of the form $\nabla \cdot (\mathbf{u}\zeta)$, where ζ is a scalar function of position, is accomplished by a combination of conservative full donor cell [21] and interpolated donor cell [24] differencing, typically 20 and 80 %, respectively.

4. Field Calculations

The field calculations generate the self-consistent electric and magnetic fields in the radiation-free limit [15]. This limit is achieved by solving the following equations:

$$\begin{aligned} &\nabla \cdot \mathbf{E}_l = 4\pi e(n_i - n_e), && \nabla \times \mathbf{E}_l = 0, \\ &\nabla \cdot \mathbf{E}_t = 0, && \nabla \times \mathbf{E}_t = -\frac{1}{c}\frac{\partial \mathbf{B}}{\partial t}, \\ &\nabla \cdot \mathbf{B} = 0, && \nabla \times \mathbf{B} = \frac{4\pi}{c}\mathbf{J} + \frac{1}{c}\frac{\partial \mathbf{E}_l}{\partial t} \end{aligned} \tag{28}$$

in which the electric field has been decomposed into longitudinal $\mathbf{E}_l$ and transverse $\mathbf{E}_t$ parts in the same manner as the electron current was decomposed in Eq. (8). The set of Eqs. (28) differs from Maxwell's equations only in that the transverse part of the displacement current $\partial \mathbf{E}_t/\partial t$ has been neglected. Working in the Coulomb gauge, Eqs. (28) may be expressed in terms of the scalar and vector potentials, ϕ and $\mathbf{A}$, respectively, as

$$\nabla^2 \phi = -4\pi e(n_i - n_e), \tag{29}$$

$$\nabla^2 \mathbf{A} = -(4\pi/c)\,\mathbf{J}_t\,, \tag{30}$$

$$\nabla^2 \mathbf{E}_t = (4\pi/c^2)\,\dot{\mathbf{J}}_t\,, \tag{31}$$

where

$$\mathbf{B} = \nabla \times \mathbf{A} \tag{32}$$

and

$$E_l = -\nabla\phi. \tag{33}$$

The relation $\mathbf{E}_t = -(1/c)\dot{\mathbf{A}}$ is not required in this formulation of the field equations although it has been used in obtaining Eq. (31). The use of the quantity $\mathbf{J}_t$ in Eq. (30) for $\mathbf{J} + (1/c)\,\partial \mathbf{E}_l/\partial t$ requires that the boundary condition used in determining the

transverse part of a vector field be the same as that desired for $\partial \mathbf{E}_t/\partial t$. Such has been the case in the present work where simple periodic and Neumann boundary conditions are used. More general boundary conditions would require that special care be taken to insure consistency in this respect.

The fundamental difference between the field calculations used here and those documented by Nielson and Lewis [15] is that Eq. (29) cannot be used to find the scalar potential in the quasineutral limit. An alternative method for determining ϕ can be found by summing the electron and ion momentum equations [16, 17]. The resulting equation is

$$(4\pi/c^2)(\dot{\mathbf{J}}_i + \dot{\mathbf{J}}_e) = (\mathbf{D} + \mu(\mathbf{E}_i + \mathbf{E}_t) + \xi \times \mathbf{B}), \tag{34}$$

where

$$\mu = \frac{4\pi q^2 n}{c^2}\left(\frac{1}{m_i} + \frac{1}{m_e}\right), \tag{35}$$

$$\xi = \frac{4\pi e}{c^3}\left(\frac{\mathbf{J}_i}{m_i} - \frac{\mathbf{J}_e}{m_e}\right), \tag{36}$$

$$\mathbf{D} = \frac{4\pi}{c^2}(\mathbf{K}_i + \mathbf{K}_e), \tag{37}$$

and $\mathbf{K}_i$ is the divergence of the ion kinetic energy tensor, the ion counterpart of Eq. (16), accumulated in the ion particle advancing section of the model. Taking the divergence of both sides of Eq. (34) and solving for μE_i gives

$$\nabla \cdot (\mu \nabla\phi) = \nabla \cdot (\mathbf{D} + \mu \mathbf{E}_t + \xi \times \mathbf{B}) \tag{38}$$

in which the definition given by Eq. (33) is used. In deriving Eq. (38), use has been made of the fact that the divergence of the left side of Eq. (34) vanishes as a result of quasineutrality, a consequence easily understood by taking the time derivative of Eq. (7).

Equation (38) serves the same purpose for the quasineutral hybrid model as Poisson's equation serves for other models not requiring quasineutrality. In particular, since μ as defined by Eq. (35) is completely determined by the ion density, Eq. (38) and suitable boundary conditions uniquely determine the electrostatic potential throughout the simulation region. The solution can be obtained by any one of several elliptic equation solution methods; the present choice is an alternating direction implicit method due to Miller [25].

The magnetic field calculation, accomplished by solving Eqs. (30) and (32), presents no major difficulties. With proper application of boundary conditions on the vector potential (see Section 5), any externally applied magnetic field can be modeled. Additionally, boundary conditions must be specified in order to obtain the transverse part of the total current needed for the right-hand side of Eq. (30). This is accomplished for the total current, as it is for the time derivative of the electron current in Eq. (17), by subtraction of the longitudinal part. The decomposition is obtained from

$$\mathbf{J}_t = \mathbf{J} + \nabla V, \tag{39}$$

where

$$\nabla^2 V = -\nabla \cdot \mathbf{J} \tag{40}$$

in which the boundary conditions on V are determined by specifying the normal component of $\mathbf{J}_l$ on the simulation boundaries as discussed in the next section.

The $\mathbf{E}_t$ calculation is somewhat more complicated than the preceding calculation of the magnetic field. It has been demonstrated that the calculation of $\mathbf{E}_t$ needs to be fully implicit in time [15] since this model exhibits instantaneous propagation. To avoid finite differencing in time, it is therefore necessary to obtain the time derivative of the total current by summing the ion and electron momentum equations which results in

$$4\pi \dot{\mathbf{J}} = \mathbf{D} + \mu(\mathbf{E}_l + \mathbf{E}_t) + \xi \times \mathbf{B}, \tag{41}$$

where μ, ξ, and $\mathbf{D}$ are defined by Eqs. (35), (36), and (37), respectively. Obtaining $\dot{\mathbf{J}}_{et}$ from $\dot{\mathbf{J}}_e$ is accomplished using the same procedure used for the right-hand side of the vector potential calculation Eq. (30), namely, by subtracting off the longitudinal part. This is expressed by

$$4\pi \dot{\mathbf{J}}_t = 4\pi(\dot{\mathbf{J}} - \dot{\mathbf{J}}_l) = 4\pi(\dot{\mathbf{J}} + \nabla V) \tag{42}$$

for which V is generated by

$$\nabla^2 V = -\nabla \cdot \dot{\mathbf{J}} \tag{43}$$

with the boundary conditions on V determined by specifying the normal component of $\dot{\mathbf{J}}$ on the simulation boundaries. Since the right-hand side requires an explicit expression of $\mathbf{E}_t$, a fully implicit calculation of $\mathbf{E}_t$ requires iteration. To this end, the rapidly converging iteration scheme described by Nielson and Lewis [15] is implemented to provide the solution to Eq. (31).

One additional complication is that the quasineutral Poisson equation, Eq. (38), requires $\mathbf{E}_t$ as a source term and the equation for $\mathbf{E}_t$, Eq. (31) with source given by Eq. (42), requires $\mathbf{E}_l$ as a source term. A fully implicit solution requires, therefore, iteration over both $\mathbf{E}_l$ and $\mathbf{E}_t$ calculations. In practice, the code runs stably with two or three iterations over both E_l and E_t calculations.

5. Boundary Conditions

As indicated in Section 1, hybrid simulation methods are expected to model not only strongly inhomogeneous macroscopic plasma properties but also the plasma interaction with the geometric configuration of the plasma vessel and/or external fields. Therefore some discussion of the mechanisms through which the simulated plasma interacts with its environment are in order. Obviously this section cannot be complete because of the extreme problem dependence of these issues. An attempt is made only to identify those mechanisms though which the model may interact with external influences.

The initialization of the plasma representation must specify a major part of the

desired geometric configuration. In addition to all the boundary conditions required at any other time, the initialization also requires specifying the initial position and velocity of each ion as well as the two-dimensional spatial dependence of the electron temperature T_e and each component of the electron transverse current $\mathbf{J}_{et}$. To complete the initialization, the self-consistent fields and the longitudinal electron current $\mathbf{J}_{el}$ need to be constructed. The boundary conditions required to accomplish these tasks are also required on all successive time steps.

The required boundary conditions model external interactions of three types: the explicit boundary conditions applied to field solutions, the treatment of ion simulation particles when they strike a boundary, and the specification of electron current boundary conditions in the various electron advance equations.

The electromagnetic field and ion simulation particle boundary conditions are relatively straightforward and are handled in a manner quite similar to that used in full-particle simulations. The fields at the boundary presumably represent imposed external fields which are approximated in some convenient way. In the present work the conditions used are periodic in y and Neumann in x. The treatment of the ion simulation particles at a boundary is usually a substitute for using a larger simulation region. For example, particles may be absorbed, reflected, or reemitted with some new velocity distribution. The choice for the present work is perfect reflection.

The boundary condition on the electron current components may need to reflect the fact that external currents flow through the simulation region. A transverse or divergence-free contribution to the electron current from external effects can appear in two ways. The first is by means of the initial value of $\mathbf{J}_{et}$ (which is not a true boundary condition), while the second is a possibly time-varying boundary condition on the $\dot{\mathbf{J}}_{et}$ calculation described by Eqs. (18) and (19). The boundary condition needed for this calculation is the time derivative of the normal component of $\dot{\mathbf{J}}_{el}$ on the simulation surface, which is obtained by taking the derivative with respect to time of the boundary condition on $\mathbf{J}_{el}$ already specified for Eq. (14).

Finally, the boundary conditions required to construct the right-hand sides of the elliptic equations for $\mathbf{A}$ and $\mathbf{E}_t$, Eqs. (30) and (31), respectively, require the same vector decomposition procedures. The difference is that the source terms that must now be decomposed are the sum of the electron and ion currents. These boundary conditions are in fact specified by those already imposed on the electron current solutions in Eqs. (14) and (19) and on the ion current by the particle boundary algorithm.

The constraints that must be considered when applying these boundary conditions are that since the divergence of the quantities $\mathbf{J}_l$, $\dot{\mathbf{J}}_l$, $\mathbf{J}_{el}$, $\dot{\mathbf{J}}_{el}$, $\mathbf{B}$, $\mathbf{E}_l$, and $\mathbf{E}_t$ are all zero or assumed small, the surface integral

$$\int_s \mathbf{F} \cdot d\mathbf{s} \tag{44}$$

must vanish where $\mathbf{F}$ is any one of these quantities. The interpretation is obvious: in this model, there can be no net source or sink for any current, electric field, or magnetic field within the simulation region.

6. Results

One-dimensional tests of the model provided initial verifications that selected physical phenomena could be represented by this model [16]. However, one-dimensional calculations with this model, indeed any nonradiative Darwin model, are considerably simpler than calculations in two or more dimensions. The relative simplicity in one dimension is due to the ease with which vectors can be decomposed into longitudinal and transverse components when gradients are allowed in only one direction. In two or more dimensions, more general techniques are always required for vector decomposition. The techniques described in preceding sections have succeeded to the extent that good agreement between this hybrid model and a conventional particle-in-cell model (particle ions and particle electrons) has been obtained for strongly inhomogeneous two-dimensional plasma simulations. The test problem used for this comparision is the temporal evolution of the lower-hybrid-drift (LHD) unstable equilibrium [17, 18].

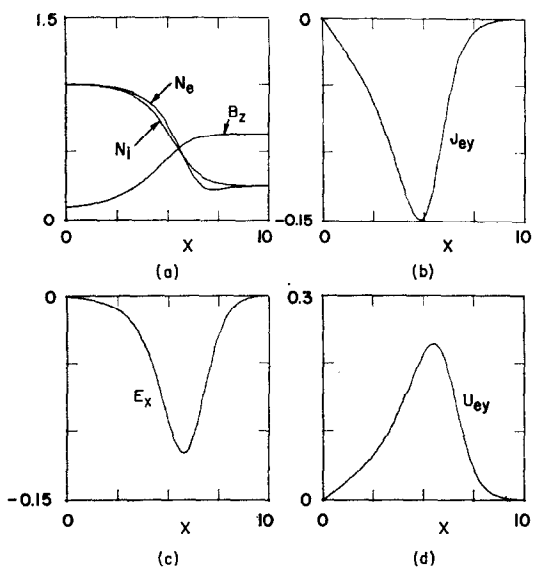

FIG. 1. Profiles of the unstable Vlasov equilibrium used to initialize the two simulations for $0 \leqslant x \leqslant 10c\omega_{pe}^{-1}$. The equilibrium is homogeneous in y. Shown as a function of x are (a) the ion density n_i, electron density n_e, and the z component of the magnetic field $\mathbf{B}_z$, (b) the y component of the electron current $\mathbf{J}_{ey}$, (c) the electrostatic field $\mathbf{E}_x$, and (d) the electron drift velocity $\mathbf{u}_{ey}$. The densities are normalized to unity at $x = 0$, while the electric and magnetic fields are measured in units of $m_e\omega_{pe}c/e$.

The LHD unstable equilibrium [26] chosen for the initialization has features suitable for both types of simulation. The equilibrium must have a sufficiently narrow sheath region to insure a substantial LHD growth rate so that the instability can be clearly distinguished from the inherent noise of particle methods. However, the sheath

must not be so thin as to require deviations from charge neutrality which tax the quasineutral assumption of this hybrid model. The Vlasov equilibrium [26] used to initiate the full-particle simulation in this study is shown in Fig. 1. The deviation from charge neutrality can be expressed, using Poisson's equation, by noting that

$$\frac{dE_x/dx}{n_i} \leqslant 0.2 \tag{45}$$

for $0 < x < x_{\max}$ and that the extreme value of this relation occurs only in a small localized region. The temporal evolution of the LHD instability using the full-particle code is best displayed by the B_z contours shown in Fig. 2 which clearly show the development of flute structures. The wavelength of these flutes is on the order of five electron gyroradii and the growth time is approximately $100\omega_{pe}^{-1}$.

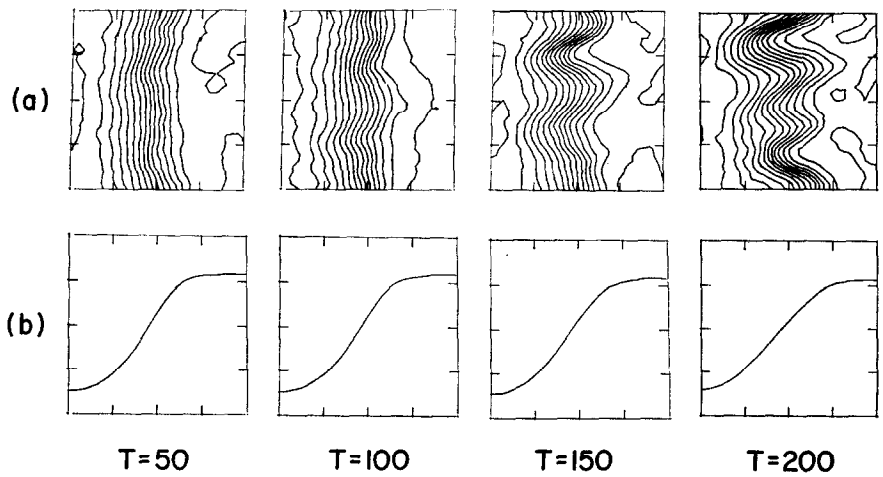

FIG. 2. Full-particle simulation of the time evolution of the magnetic field component $\mathbf{B}_z$ starting from the equilibrium shown in Fig. 1. The x-y contours of $\mathbf{B}_z$ for $0 \leqslant x \leqslant 10c\omega_{pe}^{-1}$ and $0 \leqslant y \leqslant 20c\omega_{pe}^{-1}$ are shown in (a), while the y-averaged profile of $\mathbf{B}_z$ is shown in (b).

The equilibrium for the hybrid code is deduced from the Vlasov equilibrium shown in Fig. 1 by setting $n_e = n_i$. This is mathematically equivalent to assuming dE_x/dx is small compared to n_i. This assumption also modifies the pressure balance relation used to obtain P_{xx} in effect suppressing the fact that the E^2 energy is much exact hybrid equilibrium which corresponds more and more closely to the Vlasov equilibrium as the sheath becomes broader and consequently dE_x/dx goes to zero. The temporal evolution of the B_z contours of this equilibrium as given by the two-dimensional hybrid code QN2 is shown in Fig. 3.

Comparing Figs. 2 and 3, it is apparent that both the growth rate and wavelength are nearly the same. Such agreement between the two techniques in this strongly

inhomogeneous configuration with nontrivial two-dimensional effects demonstrates, at a minimum, that the physical effects required for this instability are still present in the new model. In addition, with the initial plasma gradients requiring such a significant E_x to maintain equilibrium, it is interesting to note that the quasineutral Poisson equation, Eq. (38), produces substantially the same E_x for the hybrid code as does the true Poisson equation for the full-particle code. The enhanced diffusion, evident in the low density region in the hybrid run (Fig. (3)), is presently under investigation. Preliminary indications are that the difficulty is related to the exact form of the differencing scheme for Eqs. (21) and (22) and to the excessive fluctuations caused by a very small number of simulation particles in the low density region.

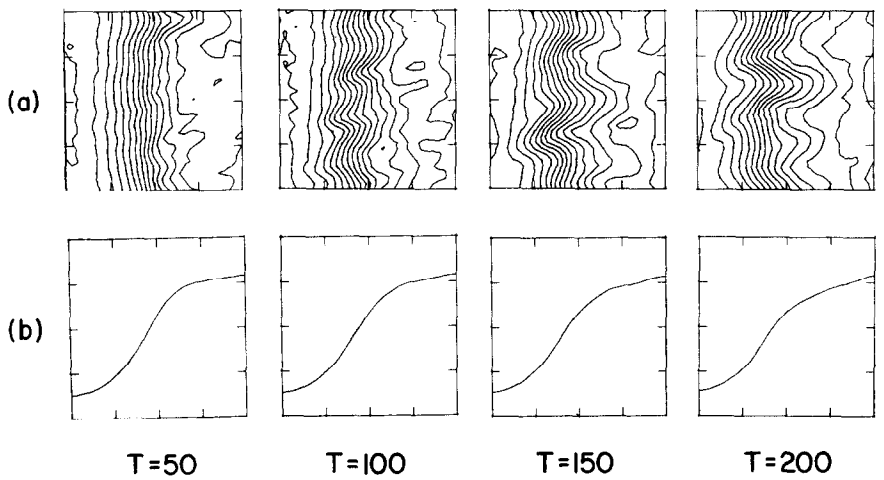

FIG. 3. Hybrid simultations of the time evolution of $\mathbf{B}_z$ with all parameters the same as the full-particle simulation shown in Fig. 2. Comparison of the results of the two simulation techniques reveals very similar wavelength and growth rate for the developing flutes.

No attempt has been made in these two-dimension tests to exploit the larger time step capability of the hybrid model; the primary purpose of the work presented here is to demonstrate agreement between the full particle-in-cell model and the hybrid model. An inhomogeneous equilibrium has been selected with properties which are appropriate for the comparison. Consequently, in these comparison runs the equilibrium electron drift velocity is sufficiently large that the limiting factor on the time step is $\Delta t \leqslant \Delta y/u_{ey}$ since flow must be less than one cell per time step.

For the comparisons given here the particle-in-cell results (Fig. 2) were obtained with $\Delta t = 0.2\omega_{pe}^{-1}$, 12 800 each of ions and electrons, 32 cells in both x and y with $0 \leqslant x \leqslant 10c/\omega_{pe}$ and $0 \leqslant y \leqslant 20c/\omega_{pe}$. The hybrid results (Fig. 3) were obtained with $\Delta t = 0.5\omega_{pe}^{-1}$ and 12 800 ions. The cell sizes and numbers as well as the equilibrium parameters were the same. In both cases the magnetic field $\mathbf{B}_z$ in units of $m_e\omega_{pe}c/e$ is about 0.7 in the low density region.

7. Conclusion

A quasineutral hybrid model has been presented which combines a full kinetic treatment of the ions with a fluid treatment of the electrons. The model retains electron gyromotion effects while excluding electron plasma oscillations. The most significant new feature of the model is a quasineutral Poisson equation which determines the electrostatic field. A two-dimensional code QN2 has been written to implement this model; one- and two-dimensional tests with this code have verified all essential features of the model. Further numerical refinements will allow application to a wide range of physically important problems.

Appendix

The simulation model presented in this paper is designed to ignore some higher-frequency electron plasma phenomena such as plasma oscillations and upper hybrid waves while retaining other finite electron mass effects such as lower hybrid waves. The numerical techniques required to accomplish these ends were developed in a somewhat heuristic and empirical manner. It is desirable to have a more precise demonstration of which plasma phenomena are and are not retained in this relatively complex model. The full multidimensional model contains many more terms than can be readily analyzed. However, indications of the time scales important to this model can be obtained by eliminating some of the variables and restricting the dimensionality.

In the analysis which follows, it is assumed that $T_e = T_i = T\,(= \text{const})$, resistivity is zero, the model has spatial variation in only one direction ($\mathbf{k} = k\mathbf{e}_x$), and the plasma under consideration has no zeroth-order gradients (and therefore no zeroth-order drift velocities in either ions or electrons). The basic equations for the electron fluid and the Darwin fields are Eqs. (13)–(31), and (35). The ions can be adequately represented for present purposes by the first two velocity moments. Equations governing the first-order magnetic field components are unnecessary for linear analysis in the limit of vanishing zeroth-order gradients. After linearization and assuming all first-order quantities have the usual $\exp(ikx + i\omega t)$ space and time dependences, the following equations form the basis of the linear dispersion relations which will be developed.

$$\omega n = -kn_0 u_{ix}\,, \tag{A1}$$

$$u_{ex} = u_{ix}\,, \tag{A2}$$

$$\left(i\omega \mathbf{u}_e = -\frac{e}{m_e}\mathbf{E} - \mathbf{u}_e \times \boldsymbol{\omega}_{ce}\right) \times \mathbf{e}_x\,, \tag{A3}$$

$$\left(i\omega \mathbf{u}_i = \frac{e}{m_i}\mathbf{E} + \mathbf{u}_i \times \boldsymbol{\omega}_{ce}\right) \times \mathbf{e}_x\,, \tag{A4}$$

$$-\mu E_x = \frac{4\pi e}{c^2}\left[ik\frac{(m_i - m_e)}{m_i m_e}nT + n_0(\mathbf{u}_i \times \boldsymbol{\omega}_{ci} + \mathbf{u}_e \times \boldsymbol{\omega}_{ce}) \cdot \mathbf{e}_x\right], \tag{A5}$$

$$\left[-k^2\mathbf{E} = \mu\mathbf{E} + \frac{4\pi e}{c^2} n_0(\mathbf{u}_i \times \boldsymbol{\omega}_{ci} + \mathbf{u}_e \times \boldsymbol{\omega}_{ce})\right] \times \mathbf{e}_x , \tag{A6}$$

$$\boldsymbol{\omega}_{cj} = \frac{e\mathbf{B}_0}{m_j c}, \qquad j = \text{particle type.} \tag{A7}$$

The density n_0 and the magnetic field $\mathbf{B}_0$ are the only nonvanishing zeroth-order quantities. μ is given by Eq. (35).

First, waves propagating perpendicular to the zeroth-order magnetic field $\mathbf{B}_0 = B_0\mathbf{e}_z$ are considered. Hence, $\boldsymbol{\omega}_{ce} = \omega_{ce}\mathbf{e}_z$, $\boldsymbol{\omega}_{ci} = \omega_{ci}\mathbf{e}_z$ which for this problem implies $\mathbf{k} \cdot \mathbf{B}_0 = 0$ and after some algebra, all variables except the electric field components are eliminated. Setting the determinant of coefficients to zero to find nontrivial solutions, it is found that

$$\omega^2 = \omega_{ce}\omega_{ci} \frac{c^2k^2}{c^2k^2 + \omega_{pi}^2 + \omega_{pe}^2} + c_s^2k^2 \frac{m_i - m_e}{m_i + m_e} \tag{A8}$$

and

$$c^2k^2 + \omega_{pe}^2 + \omega_{pi}^2 = 0, \tag{A9}$$

where c_s^2 is the ion sound velocity squared given by

$$c_s^2 = T/m_i . \tag{A10}$$

Equation (A9) simply represents the evanescent transverse wave which is a consequence of the Darwin model. In this case ($B_0\mathbf{e}_z$ and $k\mathbf{e}_x$), it arises from the decay of E_z with x. In the limit of $m_i \gg m_e$ and $\omega_{pe}^2 \gg c^2k^2$, Eq. (A8) becomes

$$\omega^2 = \frac{\omega_{ci}^2}{\omega_{pi}^2} c^2k^2 + c_s^2k^2 \tag{A11}$$

which in terms of the Alfvén velocity ($v_a^2 = B_0^2/(4\pi n_0 m_i)$) is the familiar

$$\omega^2 = (v_a^2 + c_s^2)\, k^2. \tag{A12}$$

Thus for $\mathbf{k} \cdot \mathbf{B}_0 = 0$, there are no remaining electron high-frequency phenomena on length scales much greater than c/ω_{pe} assuming realistic mass ratios. The only waves present in this limit are Alfvén and ion accoustic modes.

Now consider waves propagating parallel to the zeroth-order magnetic field. The one-dimensional spatial variation is still considered to be the x-direction but the external $\mathbf{B}$ field is now given as $\mathbf{B}_0 = B_0\mathbf{e}_x$ so that $\boldsymbol{\omega}_{ce} = \omega_{ce}\mathbf{e}_x$ and $\boldsymbol{\omega}_{ci} = \omega_{ci}\mathbf{e}_x$ implying $\mathbf{k} \cdot \mathbf{B}_0 \neq 0$. Substituting these parameters into Eqs. (A1)–(A7) and eliminating variables until only the electric field components remain, the coefficient of the unknowns is again set to zero to find nontrivial solutions. The result is

$$(\omega \mp \omega_{ce})(\omega \pm \omega_{ci}) \pm \frac{\omega_{pe}^2\omega_{ce}(\omega \pm \omega_{ci}) - \omega_{pi}^2\omega_{ci}(\omega \mp \omega_{ce})}{c^2k^2 + \omega_{pi}^2 + \omega_{pe}^2} = 0 \tag{A13}$$

for circularly polarized transverse waves ($\mathbf{k} \cdot \mathbf{E} = 0$) and

$$\omega^2 = \frac{(m_i - m_e)}{(m_i + m_e)} c_s^2 k^2 \tag{A14}$$

for longitudinal waves ($\mathbf{k} \cdot \mathbf{E} \neq 0$). In the limit of $m_i \gg m_e$ and for frequencies $\omega \gg \omega_{ci}$, Eqs. (A13) and (A14) become

$$\omega = \pm\omega_{ce}\left(1 - \frac{\omega_{pe}^2}{c^2k^2 + \omega_{pe}^2}\right), \tag{A15}$$

$$\omega^2 = c_s^2 k^2. \tag{A16}$$

Therefore, this model retains electron cyclotron oscillations for those mode components for which $\mathbf{k} \cdot \mathbf{B} \neq 0$.

In the numerical simulation model, care must be taken to keep Δt a small fraction of the inverse of the highest frequency expected. Studies with the coded version of this model verify that, as long as there are no components of **B** in the two-dimensional simulation plane, the absolute stability limit on the magnitude of Δt is given by $\Delta t \leqslant 1.3/(\omega_{ci}\omega_{ce})^{1/2}$. When there is a component of **B** in the plane of simulation, the upper bound on Δt is reduced to $\Delta t \leqslant 1.6/\omega_{ce}$ where ω_{ce} is given by Eq. (A7) evaluated by substituting for **B** the value of $(\mathbf{k} \cdot \mathbf{B})/k$.

ACKNOWLEDGMENTS

The initial work on the development of this model, as reported in Ref. [15], was in collaboration with Dr. D. Winske whose contribution is gratefully acknowledged. The authors also benefitted from discussions with Drs. D. A. Barnes, J. U. Brackbill, J. E. Dendy, J. P. Freidberg, and A. G. Sgro. This work was performed under the auspices of the USERDA.

REFERENCES

1. H. GRAD, *Phys. Fluids* **4** (1961), 1366.
2. D. A. D'IPPOLITO AND R. C. DAVIDSON, *Phys. Fluids* **18** (1975), 1507.
3. J. P. FREIDBERG, *Phys. Fluids* **19** (1972), 1102.
4. J. P. FREIDBERG AND D. W. HEWETT, *Phys. Fluids*, **20** (1977), 2128.
5. H. R. LEWIS AND L. TURNER, *Nuclear Fusion* **16** (1976), 993.
6. R. A. GERWIN, The Vlasov-Fluid Model with Electron Pressure, LA-6130-MS, 1975.
7. K. HAIN, G. HAIN, K. V. ROBERTS, S. J. ROBERTS, AND W. KOPPENDORFER, *Z. Naturforsch.* **15A** (1960), 1039.
8. P. C. LEWIER AND N. A. KRALL, *Phys. Fluids* **16** (1973), 1953.
9. A. G. SGRO AND C. W. NIELSON, *Phys. Fluids* **19** (1976), 126.
10. S. HAMASAKI AND N. A. KRALL, *Phys. Fluids* **20** (1977), 229.
11. C. R. SHONK AND R. L. MORSE, Proceedings of the APS Topical Conference on Numerical Simulation of Plasmas, Los Alamos, New Mexico, 1968, paper C3.
12. J. A. BYERS, B. I. COHEN, W. C. CONDIT, AND J. D. HANSON, *J. Comp. Phys.* **27** (1978), 363.

13. D. W. Forslund and J. P. Freidberg, *Phys. Rev. Lett.* **27** (1971), 1189.
14. P. C. Liewer, Proceedings of the Seventh Conference on Numerical Simulation of Plasmas, N.Y.U., 1975.
15. C. W. Nielson and H. R. Lewis, "Particle-Code Models in the Nonradiative Limit," Methods in Computational Physics, Vol. 16, p. 367, Academic Press, New York, 1976.
16. C. W. Nielson, D. Winske, and D. W. Hewett, Proc. Meet, on Th. Aspects of CTR, 1976, paper 2a-17.
17. D. W. Hewett, C. W. Nielson, and D. Winske, *Bull. Amer. Phys. Soc.* **21** (1976), 1038.
18. D. Winske and D. W. Hewett, *Phys. Rev. Lett.* **35** (1975), 937.
19. C. L. Longmire, "Elementary Plasma Physics," p. 21, John Wiley and Sons, New York, 1963.
20. L. D. Landau and E. M. Lifshitz, "Fluid Mechanics," p. 4, Addison–Wesley, Reading, Mass., 1959.
21. C. W. Hirt, *J. Computational Phys.* **2** (1968), 339.
22. J. P. Boris and D. L. Book, "Solution of Continuity Equations by the Method of Flux-Corrected Transport," Methods in Computational Physics, Vol. 16, p. 85, Academic Press, New York, 1976.
23. P. J. Roache, "Computational Fluid Dynamics," Hermosa Publishers, Albuquerque, 1976.
24. A. A. Amsden and C. W. Hirt, YAQUI: An Arbitrary Lagrangian-Eulerian Computer Program for Fluid Flow at All Speeds, LA-5100, 1973, p. 10.
25. K. Miller, Seminar at Los Alamos Scientific Laboratory, April 8, 1976.
26. D. W. Hewett, C. W. Nielson, and D. Winske, *Phys. Fluids* **19** (1976), 443.